Note: This copy is for your personal non-commercial use only. To order presentation-ready copies for distribution to your colleagues or clients, contact us at www.rsna.org/rsnarights.

A Receptor-targeted Fluorescent Radiopharmaceutical for Multireporter Sentinel Lymph Node Imaging[1]

Derek K. Emerson, MD
Karl K. Limmer, MD
David J. Hall, PhD
Sung-Ho Han, PhD
William C. Eckelman, PhD
Christopher J. Kane, MD
Anne M. Wallace, MD
David R. Vera, PhD

Purpose: To determine the imaging and receptor-binding properties of a multireporter probe designed for sentinel lymph node (SLN) mapping via nuclear and fluorescence detection.

Materials and Methods: The animal experiments were approved by the institutional animal care and use committee. A multireporter probe was synthesized by covalently attaching cyanine 7 (Cy7), a near-infrared cyanine dye, to tilmanocept, a radiopharmaceutical that binds to a receptor specific to recticuloendothelial cells. In vitro binding assays of technetium 99m (^{99m}Tc) -labeled Cy7 tilmanocept were conducted at 4°C by using receptor-bearing macrophages. Optical SLN imaging after foot pad administration was performed by using two molar doses of Cy7 tilmanocept. Six mice were injected with 0.11 nmol of ^{99m}Tc-labeled Cy7 tilmanocept (low-dose group); an additional six mice were injected with 31 nmol of ^{99m}Tc-labeled Cy7 tilmanocept (high-dose group) to saturate the receptor sites within the SLN. After 2.5 hours of imaging, the mice were euthanized, and the sentinel and distal lymph nodes were excised and assayed for radioactivity for calculation of SLN percentage of injected dose and extraction. Four mice were used as controls for autofluorescence. Standard optical imaging software was used to plot integrated fluorescence intensity against time for calculation of the SLN uptake rate constant and scaled peak intensity. Significance was calculated by using the Student *t* test.

Results: In vitro binding assays showed subnanomolar affinity (mean dissociation constant, 0.25 nmol/L ± 0.10 [standard deviation]). Fluorescence imaging showed a detection sensitivity of 1.6 $\times 10^3$ counts · sec^{-1} · μW^{-1} per picomole of Cy7. All four imaging metrics (percentage of injected dose, SLN extraction, SLN uptake rate constant, and expected peak fluorescence intensity) exhibited higher values ($P = .005$ to $P = .042$) in the low-dose group than in the high-dose group; this finding was consistent with receptor-mediated image formation.

Conclusion: The multireporter probe ^{99m}Tc-labeled Cy7 tilmanocept exhibits in vitro and in vivo receptor-binding properties for successful receptor-targeted SLN mapping with nuclear and optical imaging.

©RSNA, 2012

Supplemental material: *http://radiology.rsna.org/lookup/suppl/doi:10.1148/radiol.12120638/-/DC1*

[1] From the Moores UCSD Cancer Center (D.K.E., K.K.L., D.J.H., S.H.H., C.J.K., A.M.W., D.R.V.), Department of Radiology (D.J.H., S.H.H., W.C.E., D.R.V.), Department of Surgery (D.K.E., K.K.L., C.J.K., A.M.W.), and UCSD In Vivo Cancer and Molecular Imaging Center (D.J.H., S.H.H., W.C.E., D.R.V.), University of California, San Diego, 3855 Health Sciences Dr, La Jolla, CA 92093. Received March 27, 2012; revision requested April 24; revision received May 8; accepted May 23; final version accepted June 5. **Address correspondence to** D.R.V. (e-mail: *dvera@ucsd.edu*).

©RSNA, 2012

Sentinel lymph node (SLN) mapping (1) of breast cancer (2,3) and melanoma (4) is well validated (5–7) and has become standard procedure in the determination of whether these cancers have metastasized to regional lymph nodes. The sentinel node concept is based on the hypothesis (8) that lymphatic spread of metastatic cells within a lymph node basin proceeds in an orderly fashion through multiple anatomic levels. If the SLN, which is the first lymph node that drains the tumor, is free of cancer cells, then the remaining lymph nodes in the chain will also be free of metastatic disease. For a patient with breast cancer, if the SLN is negative, the remaining lymph nodes within the axillary basin need not be removed, thereby reducing the risk of lymphedema (9). In patients with melanoma, disease-free SLNs offer a strong prognostic indication of survival (10).

Technetium 99m (^{99m}Tc)-labeled tilmanocept, also known as ^{99m}Tc diethylenetriaminepentaacetic acid mannosyl dextran (11) and Lymphoseek (12) (Navidea Biopharmaceuticals, Dublin, Ohio), is a glycoconjugate with high affinity to the receptor mannose binding protein, which is specific to recticuloendothelial cells. The relatively small size of the molecule (<8 nm) enables it to rapidly enter the lymphatic system after intradermal injection (12,13). The specific interaction of ^{99m}Tc tilmanocept with the receptor permits the molecule to accumulate within the SLN, with minimal passage into distal lymph nodes. Phase I clinical trials in patients with breast cancer (12) and in those with melanoma (13) successfully demonstrated these properties, which were confirmed in phase II (14) and phase III (15) clinical trials.

Advance in Knowledge

- The multireporter probe fluorescent-labeled technetium 99m (^{99m}Tc) tilmanocept exhibits receptor-mediated accumulation by sentinel lymph nodes (SLNs) at a concentration that is visible with fluorescence and nuclear imaging.

Rapid accumulation and long retention of tilmanocept by the SLN permits greater logistic flexibility, which is more compatible with a fluorescent tag than with a radioactive label. For example, rapid SLN uptake after submucosal injection of ^{99m}Tc tilmanocept (16) permits SLN mapping within minutes of injection into the stomach or colon. Unfortunately, intraoperative injections of radioactive material present logistical and regulatory issues. Conversely, a prolonged interval between tilmanocept administration and SLN mapping is possible due to persistent SLN retention imparted by receptor binding (17). An example would be tilmanocept injection during colonoscopy followed by surgery a week later. If radiolabeled with ^{99m}Tc, the SLN at the time of surgery would not contain a detectable amount of radioactivity. The solution to these and other scenarios is to label tilmanocept with a fluorescent reporter and perform SLN mapping with a handheld optical imaging system (18). An additional setting compatible with an optical reporter is robot-assisted surgery (19), where near-infrared-capable imaging systems are integrated into the three-dimensional viewing console (20); mapping in this setting would follow single photon emission computed tomography (SPECT) cross-sectional imaging and would enable one to localize the SLN basins within the pelvis.

The purpose of this study was to determine the imaging and receptor-binding properties of a multireporter probe designed for SLN mapping via nuclear and fluorescence detection.

Implications for Patient Care

- This fluorescent-labeled SLN mapping agent is compatible with new surgical and imaging instrumentation, such as high-bandwidth illumination and camera systems designed for near-infrared imaging
- A dual ^{99m}Tc- and fluorescent-labeled agent would permit SPECT imaging of the pelvic lymph node basins before surgery and guide SLN mapping during surgery for breast, prostate, bladder, and gynecologic cancers.
- Intraoperative optical imaging would eliminate the need to administer radioactive agents in the surgical suite during SLN mapping of gastrointestinal cancers.

Materials and Methods

Tilmanocept, the active ingredient in Lymphoseek, was provided by Navidea Biopharmaceuticals. The authors had full control over the inclusion of all data and information submitted for publication. This study was approved by the Institutional Animal Care and Use Committee of the University of California, San Diego.

Synthesis and Characterization of Optically Labeled Tilmanocept

Conjugation of the optical reporter, a cyanine dye (21), to tilmanocept proceeded in a manner described previously (22). Estimation of cyanine 7 (Cy7) density was defined as the average number of Cy7 molecules per tilmanocept molecule and was performed with a method similar to that used by Mujumbar and coworkers (21), in which they used dye

Published online before print
10.1148/radiol.12120638 **Content code:** MI

Radiology 2012; 265:186–193

Abbreviations:
ROI = region of interest
SLN = sentinel lymph node

Author contributions:
Guarantors of integrity of entire study, D.J.H., A.M.W., D.R.V.; study concepts/study design or data acquisition or data analysis/interpretation, all authors; manuscript drafting or manuscript revision for important intellectual content, all authors; approval of final version of submitted manuscript, all authors; literature research, D.K.E., K.K.L., D.J.H., A.M.W., D.R.V.; experimental studies, D.K.E., K.K.L., D.J.H., A.M.W., D.R.V.; statistical analysis, D.K.E., K.K.L., D.J.H., S.H.H., A.M.W.; and manuscript editing, D.K.E., K.K.L., D.J.H., W.C.E., C.J.K., A.M.W., D.R.V.

Funding:
This research was supported by the National Institutes of Health (grant P50 CA128346).

Potential conflicts of interest are listed at the end of this article.

absorbance at the absorption maximum to measure the quantity of cyanine dye. Absorbance and emission spectra were measured for unconjugated Cy7 and Cy7-conjugated tilmanocept preparations. Absorbance spectra were obtained at five dilutions of each Cy7 tilmanocept preparation and unconjugated Cy7. All solutions were in 0.9% saline (pH, 6.0) within a 10-mm cuvette, with all absorbances below 0.05 units. Emission spectra (710–850 nm, 5-nm slit width) (Fluorolog 2; Horiba Jobin Yvon, Edison, NJ fitted with an R928 photomultiplier tube; Hamamatsu Photonics, Iwata City, Japan) were excited at 700 nm. Absorbance spectra (Varian Carey 3E; Agilent Technologies, Walnut Creek, Calif) were acquired between 400 and 850 nm (1.5-nm slit width). Details of synthesis and Cy7 density measurements are provided in Appendix E1 (online).

Radiolabeling Cy7 Tilmanocept with ^{99m}Tc

Radiolabeling of Cy7 tilmanocept (Fig 1a) with ^{99m}Tc was performed with a tin reduction method (23). Quality control consisted of instant thin-layer chromatography and size exclusion high-performance liquid chromatography with radioactivity and fluorescence detection. Radiolabeling of Cy7 tilmanocept and high-performance liquid chromatography quality control was also conducted after 4 months of storage at 5°C. All labeling reactions resulted in radiochemical yields in excess of 98% and single components within the instant thin-layer chromatography, radioactivity, and fluorescence chromatograms (Figure E1 [online]). Details for radiolabeling and quality control are provided in Appendix E1 (online).

Measurement of Receptor Affinity

We measured the equilibrium dissociation constant of Cy7 tilmanocept by using an in vitro binding assay with J774E or J774 macrophages (24). The equilibrium dissociation constant for each assay was calculated by using LIGAND software (25), and it was displayed as a Scatchard plot (26). Because the wild-type J774 macrophages do not express mannose-binding protein, the binding studies with these cells served as negative controls of ^{99m}Tc-labeled Cy7 tilmanocept and ^{99m}Tc-labeled tilmanocept binding to macrophages. The assays were conducted at 4°C to eliminate the effect of receptor recycling. Details are provided in Appendix E1 (online).

Optical Imaging

We performed dynamic fluorescence imaging in 12 mice (weight range, 20–30 g). Six Swiss Webster mice, members of the low-dose group, were injected in the foot pad with an amount of Cy7 tilmanocept that would not saturate receptor sites within the SLN. Seven days later, a second group, designated the high-dose group, received a dose 300 times greater than that administered to the low-dose group; this was designed to saturate the receptor sites within the SLN. Imaging of each group was completed within an 18-hour period.

Prior to the injection, each mouse was anesthetized via inhalation of 2%–3% isoflurane, shaved, and placed in the supine position onto a warmed imaging stage (36°C) within the optical imager (Optix MX2; Advanced Research Technologies, Montreal, Quebec, Canada). The Cy7 setting of the imager used a 758-nm excitation laser and a pair of emission filters, a 780-nm long-pass filter and a 782-nm band-pass filter, with a 20-nm bandwidth; the pixel size was determined by the distance between each rectilinear scanning position and the line offset, which were set at 1.5 mm and 1.5 mm, respectively. During imaging, continuous anesthesia was maintained by delivery of 1%–2% isoflurane via a nose cone. A total of 7.5 μL of injectate was drawn into a 0.3-mL syringe with a fixed 28-gauge needle. Each mouse in the low-dose group received 0.11 nmol of ^{99m}Tc-labeled Cy7 tilmanocept (0.28 Cy7 per tilmanocept, 0.078 nmol of Cy7), and each mouse in the high-dose group received 31 nmol of ^{99m}Tc-labeled Cy7 tilmanocept and the same amount of Cy7 (0.078 nmol) as the low-dose group. The right hind foot pad of each mouse was injected with the entire contents of each syringe and massaged for 10 seconds. Separate scanning regions were drawn over the footpad and the SLN. Serial measurements of fluorescence intensity were acquired at the injection site and in the draining lymph node basin every 10 minutes for a total of 150 minutes. Immediately after acquisition of the last image, the mice were euthanized by inhalation of carbon dioxide gas and cervical dislocation. For each mouse, the popliteal node, which represents the SLN, and the inguinal lymph node, which is distal to the popliteal lymph node relative to the injection site, were excised, placed in plastic scintillation vials, and assayed for radioactivity. In a separate group, Swiss Webster mice (n = 4) were shaved, and imaging was performed over the popliteal lymph node. This group enabled us to measure tissue autofluorescence, which was used to predict signal-to-background ratio in a human imaging study.

After all images were acquired, a medical physicist (D.J.H., 19 years of optical imaging experience) drew a region of interest (ROI) around the SLN and footpad. Each ROI was checked by another author (D.R.V., a radiochemist with 32 years of experience in kinetic modeling of imaging data). The injection site ROI encompassed the entire foot (size range, 41–89 mm^2, mean size, 66 mm^2); the size of the SLN ROI was adjusted to encompass only the area (range, 14–24 mm^2; mean, 17 mm^2) of increased signal intensity over the lymph node. The counts from each pixel within the ROI were summed to yield an integrated fluorescence intensity for each ROI at a given time point. Time-intensity curves for each mouse study were generated by using integrated fluorescence in kilocounts as the y axis and were used to calculate the SLN accumulation rates and scaled peak fluorescence intensities. Details of each calculation are provided in Appendix E1 (online).

Detection sensitivity was defined as the scaled fluorescence intensity per mole of fluorophore within an SLN. It was calculated by using the last frame of the dynamic fluorescence imaging study and the radioactivity measurement of the SLN. For each of the mice within the low-dose group, the scaled

Figure 1

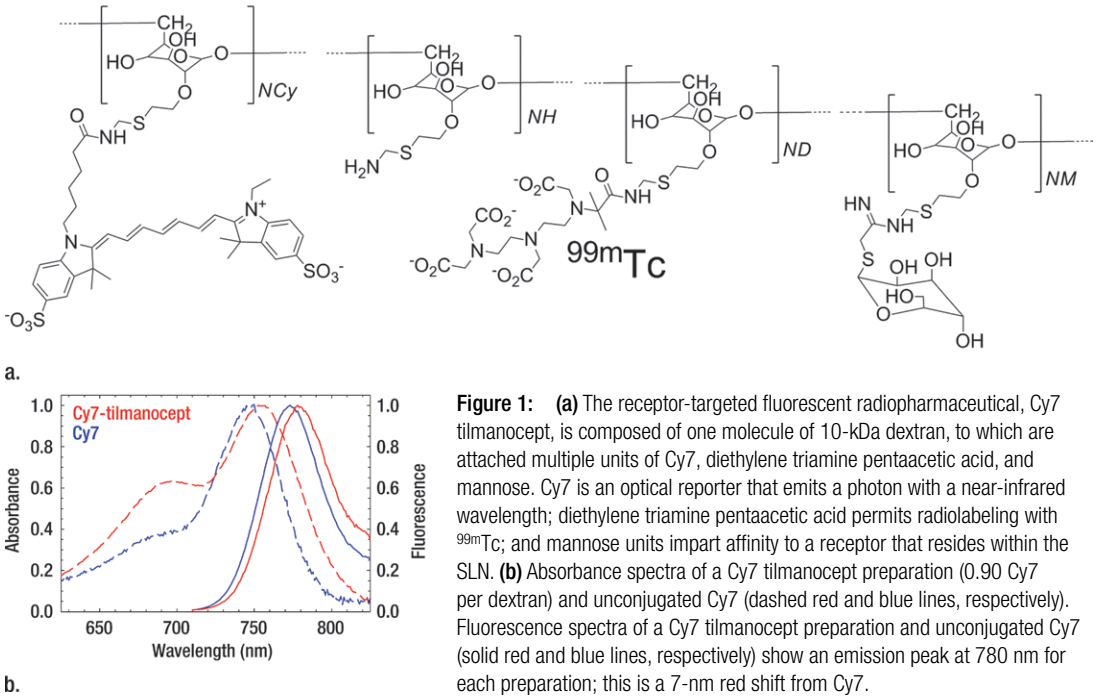

Figure 1: **(a)** The receptor-targeted fluorescent radiopharmaceutical, Cy7 tilmanocept, is composed of one molecule of 10-kDa dextran, to which are attached multiple units of Cy7, diethylene triamine pentaacetic acid, and mannose. Cy7 is an optical reporter that emits a photon with a near-infrared wavelength; diethylene triamine pentaacetic acid permits radiolabeling with ^{99m}Tc; and mannose units impart affinity to a receptor that resides within the SLN. **(b)** Absorbance spectra of a Cy7 tilmanocept preparation (0.90 Cy7 per dextran) and unconjugated Cy7 (dashed red and blue lines, respectively). Fluorescence spectra of a Cy7 tilmanocept preparation and unconjugated Cy7 (solid red and blue lines, respectively) show an emission peak at 780 nm for each preparation; this is a 7-nm red shift from Cy7.

fluorescence intensity was calculated from the SLN ROI. This value was divided by the amount of Cy7 within the SLN. The Cy7 amount was calculated by multiplying the average number of Cy7 molecules per dextran (ie, Cy7 density) by the amount of tilmanocept within the SLN, as determined with a radioactivity assay of each harvested SLN.

Nuclear Counting and Calculations

The SLNs were assayed by using a 100–200-keV window (Gamma 9000; Beckman Instruments, Fullerton, Calif) and compared with a counting standard that was prepared from a known dilution of the injected material. The percentage of injected dose of tilmanocept was calculated by comparing the tissue counts with the counting standard. Calculation of the amount of Cy7 within each SLN was based on the percentage of injected dose of tilmanocept and the measured Cy7 density of the Cy7 tilmanocept preparation. The percentage of SLN extraction was calculated as the difference between SLN and distal lymph node count rates divided by the sum of the SLN and distal lymph node count rates (11).

Statistical Analysis

We used the Student *t* test (JMP, version 9, 2010; SAS Institute, Cary NC) to calculate a one-tailed test of significance, which we justified based on our knowledge that a receptor-binding process will result in diminished accumulation when the receptor is challenged with excess ligand. We tested each of the time-intensity and time-activity metrics: SLN accumulation rates, scaled peak fluorescence intensities, percentage of injected dose, and percentage of SLN extraction. We considered a *P* value of less than .05 to indicate a significant difference. We repeated the statistical analysis by using the Wilcoxon signed rank test.

Results

Characterization of Optical and Radiochemical Properties

We synthesized two Cy7 tilmanocept preparations (Fig 1a), each with a different mean Cy7 density (0.28 and 0.90 Cy7 molecules per tilmanocept). The mouse study used the lower density preparation; the binding assays used the preparation with the 0.90 Cy7 density.

The covalent attachment of Cy7 to the amino-terminated leashes of tilmanocept altered the absorption and fluorescence spectra and slightly lowered the quantum yield. Absorbance and fluorescence spectra (Fig 1) of Cy7-conjugated tilmanocept revealed a red shift of 7 nm when compared with unconjugated Cy7. The absorbance spectra revealed an elevation of the short-wavelength shoulder compared with unconjugated Cy7 consistent with dimerization and subsequent loss of quantum yield. Quality control of ^{99m}Tc-labeled Cy7 tilmanocept that was radiolabeled 4 months after Cy7 conjugation and stored at 5°C showed single radioactivity and fluorescence peaks (Figure E1 [online]), with no evidence of free fluorophore, which has an elution volume of 12.0 mL.

Radiolabeling for the in vitro cell binding studies resulted in specific activities of 0.4×10^8 GBq/mol, without the need for purification. Moreover, high radiochemical purity (>98%) was maintained after a 240-fold dilution,

which was required to prepare the highest Cy7 tilmanocept dilution used in the cell binding assay.

Measurement of Receptor Affinity

Five ^{99m}Tc-labeled Cy7 tilmanocept binding assays at 4°C yielded a mean dissociation constant of 0.25 nmol/L ± 0.10 (standard deviation) (Table E1 [online]). This value was lower than but not significantly different from 0.42 nmol/L ± 0.31, which was the mean dissociation constant (n = 5) for ^{99m}Tc-labeled tilmanocept. The in vitro studies showed that the attachment of the optical label did not increase nonspecific binding, as shown by the fraction of nonspecific binding of the in vitro assay and the absence of binding by wild-type J774 cells, which do not express the receptor. A typical Scatchard plot of Cy7 tilmanocept binding to J774E cells is presented in Figure 2. Scatchard plots from wild-type cells did not exhibit a specific binding component.

Optical Imaging

The mean scaled fluorescence intensity of the SLNs from the six mice in the low-dose group was (0.22 ± 0.14) × 10^3 counts · sec^{-1} · μW^{-1}. The mean amount of Cy7 tilmancept within each SLN based on the ^{99m}Tc assay results was 0.44 pmol ± 0.18; by using the average value of 0.28 Cy7 molecules per tilmanocept, the mean amount of SLN Cy7 was 0.12 pmol ± 0.05. The mean detection sensitivity was (1.62 ± 0.56) × 10^3 counts · sec^{-1} · μW^{-1} per picomole of Cy7. By using an excitation power of 800 μW, mean autofluorescence intensity from the popliteal region was 516 counts ± 121 per pixel or a scaled intensity of 0.65 ± 0.15 counts · sec^{-1} · μW^{-1}.

A comparison of the SLN time-intensity curves from a low-dose study with those from a high-dose study (Fig 3) showed a receptor-mediated process for Cy7 tilmaocept accumulation by the SLN. Within minutes of injection, the large amount of tilmanocept in the high-dose study bound up all of the receptors within the SLN. Consequently, during the remainder of the study, the SLN could not accumulate any additional tilmanocept. Thus, after saturation, any tilmanocept that enters the SLN will not find a receptor to which it can bind. As a result, tilmanocept will exit and travel to the next lymph node. The result is a high-dose curve (Fig 3d) that was flat when compared with that in the low-dose study (Fig 3b). Receptor saturation resulted in lower accumulation rates, peak uptake values, percentage of injected doses, and SLN extraction coefficients. For example, the slope of the low-dose study yielded an accumulation rate constant of 1.65 $hours^{-1}$, which was 57-fold greater than the rate constant in the high-dose study.

Two metrics of SLN accumulation (Fig 4) exhibited significant differences between the two experimental groups. The Cy7 tilmanocept SLN rate constant in the low-dose group (1.36 $hours^{-1}$ ± 0.66) was significantly (P = .005) greater than that in the high-dose group (0.33 $hours^{-1}$ ± 0.34). The scaled peak fluorescence was significantly (P = .018) higher in the low-dose group (220 counts · sec^{-1} · μW^{-1} ± 140) than in the high-dose group (55 counts · sec^{-1} · μW^{-1} ± 42).

Two metrics of lymph node accumulation (Fig 5) exhibited significant differences between the two experimental groups. The mean percentage of injected dose attained with the SLNs in the low-dose group (0.40% ± 0.16) was significantly (P = .007) greater than that attained in the high-dose group (0.16% ± 0.08). The mean SLN extraction (83% ± 11) attained in the low-dose group was significantly (P = .042) greater than that attained in the high-dose group (55% ± 31). There was a significant (r = 0.85, P < .001) correlation (Figure E2 [online]) between the scaled SLN fluorescence intensity at the end of each study and the amount of SLN Cy7, as measured by ^{99m}Tc activity of each excised lymph node. The nonparametric test of significance yielded lower P values for SLN accumulation rates, scaled peak fluorescence intensities, and percentage of SLN extraction, as well as a P value of .01 for percentage of injected dose.

Figure 2

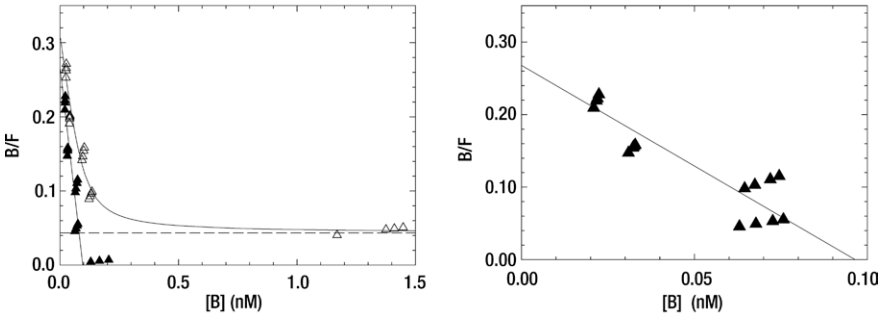

Figure 2: **(a, b)** Scatchard plots show results of a single-binding experiment analyzed with LIGAND software (25), which separated the specific- (▲) and nonspecific-bound (△) radioactivity prior to estimation of the dissociation constant. **(a)** Mean dissociation constant was 0.36 nmol/L ± 0.14 at 4°C (negative slope of straight solid line). **(b)** Expanded view of the specific-bound component used to calculate the dissociation constant of the individual assay. Mean dissociation constant of five Cy7 tilmanocept assays was 0.25 nmol/L ± 0.10, which was not significantly different from tilmanocept without Cy7 attached (0.42 nmol/L ± 0.31).

Discussion

The purpose of this study was to determine the performance of the receptor-binding fluorescent radiopharmaceutical ^{99m}Tc-labeled Cy7 tilmanocept. The nuclear and optical labels showed high stability and provided sufficient sensitivity for nuclear detection and fluorescent imaging. The receptor-binding characteristics were demonstrated in vitro at subnanomolar affinity and in vivo by receptor saturation. The specific activity achieved would permit a 3-nmol injection of 1.2 GBq, which

Figure 3

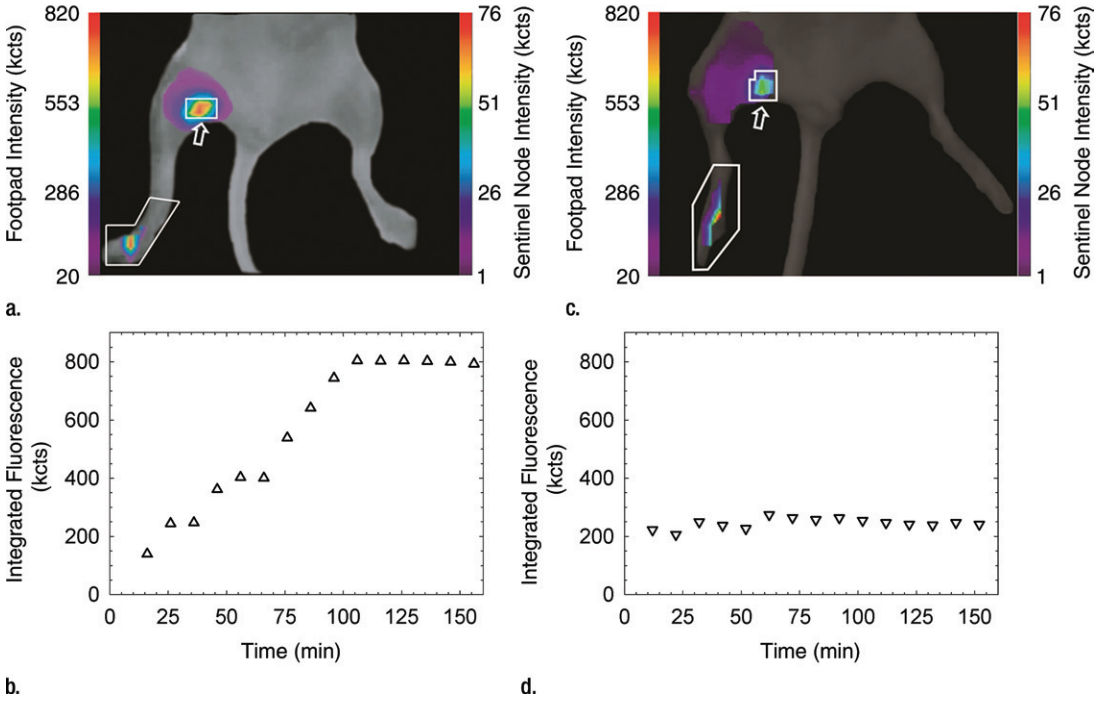

Figure 3: **(a, c)** Examples of fluorescence imaging of mouse SLNs (arrows) within ROIs (white outlines). *kcts* = Kilocounts. **(a)** Optical image obtained 150 minutes after administration of a 0.11-nmol dose of Cy7 tilmanocept yielded an SLN with an integrated fluorescence intensity with an ROI of 780 × 10^3 counts. The pixel with the highest fluorescence intensity held 64 × 10^3 counts. **(b)** Time-intensity curve from the SLN shows sustained accumulation from 140 × 10^3 counts at 15 minutes to 800 × 10^3 counts at 100 minutes. SLN uptake rate constant, percentage of injected dose, and SLN extraction were 1.65 hours^{-1}, 0.53%, and 89%, respectively. **(c)** Optical image (150 minutes) of the injection site and popliteal lymph node in a mouse in the high-dose group (31 nmol) shows decreased sentinel node intensity. **(d)** Time-intensity curve from the SLN showed diminished uptake due to receptor saturation. SLN accumulation rate, percentage of injected dose, and SLN extraction were 0.029 hour^{-1}, 0.28%, and 19%, respectively.

Figure 4

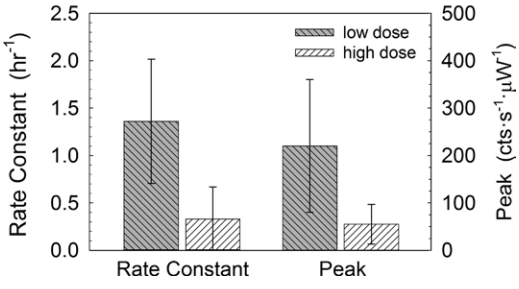

Figure 4: Box plots show mouse fluorescence imaging studies of ^{99m}Tc-labeled Cy7 tilmanocept demonstrated receptor binding to SLNs. Cy7 tilmanocept SLN uptake rate constant in the low-dose group (1.36 hours^{-1} ± 0.66) was significantly (P = .005) greater than that in the high-dose group (0.33 hours^{-1} ± 0.34). Uptake peak as measured by peak scaled fluorescence intensity was significantly (P = .018) higher in the low-dose group (220 counts · sec^{-1} · µW^{-1} ± 140) than in the high-dose group (55 counts · sec^{-1} · µW^{-1} ± 42).

Figure 5

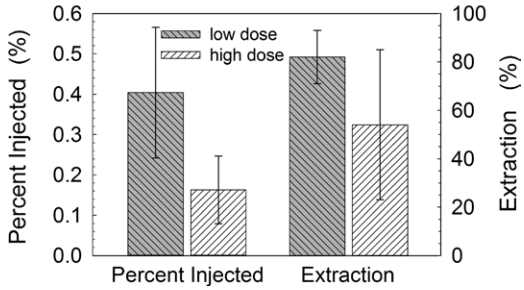

Figure 5: Box plots show radioactivity measurements that enabled us to confirm the findings of mouse fluorescence imaging studies. At 3 hours after injection, the percentage of injected dose accumulated by SLNs in the low-dose group (0.11 nmol) accumulated a significantly (P = .007) greater percentage (0.40% ± 0.16) of the injected dose than did the high-dose group (31 nmol) (0.16% ± 0.08). SLN extraction in the low-dose group (83% ± 11) was greater (P = .042) than that in the high-dose group (54% ± 31).

is over 50-fold greater than the standard dose (0.019 GBq) for a human tilmanocept SLN study (14), which uses a 3-nmol injection.

The results were consistent with the bimolecular mechanism of receptor ligand binding. The low-dose group exhibited pseudo-first-order binding of a high-specific-activity ligand, and the high-dose group exhibited second-order binding. These measurements were derived from time fluorescence curves, which exhibited dose-dependent uptake (27), which is a hallmark of in vivo receptor-mediated binding. These characteristics were demonstrated by faster accumulation rates and higher peak values for the time-fluorescence curves of the low-dose group. The fluorescence data were confirmed with nuclear measurements in the low-dose group, which exhibited higher SLN percentage of injected dose and higher SLN extraction than did the high-dose group. Also important was the fact that mean SLN accumulation in the low-dose studies was similar to the percentage of injected dose in the human ^{99m}Tc tilmanocept studies (12,13), which yielded high-quality planar images of SLNs.

The fact that the radioactive and fluorescent labels are attached to the same molecule permitted us to calculate the absolute amount of tilmanocept within each lymph node. We estimated (Appendix E1 [online]) the amount of the available SLN receptor to be approximately 50 pmol. Most important is the knowledge that a 0.11-nmol injection of Cy7 tilmanocept occupied less than 1% of the receptor population within the SLN.

The imaging studies showed that a receptor-targeted fluorescent imaging agent can yield ample signal for a clinical imaging study by using the same amount (3 nmol) of tilmanocept used for nuclear imaging (14). We conservatively estimated (Appendix E1 [online]) a signal-to-background ratio of 31-to-1 for a human imaging study with the following scenario: a 3-nmol dose of Cy7 tilmanocept bearing 1 Cy7 per tilmanocept and 0.4% SLN uptake by a 4-mm-diameter SLN 1 cm below the skin.

Recent studies have shown that fluorescent-tagged radiopharmaceuticals can provide adequate signal for fluorescence imaging. van Dam and co-workers (28) used laparoscopic fluorescence imaging of isothiocyanate-labeled folate and successfully detected ovarian cancer. This was accomplished despite the less-than-optimal nature of the fluorescent label. Van der Poel and colleagues (29) combined indocyanine green with NanoColl (GE Healthcare, Amersham Health, Braunschweig, Germany) and successfully detected SLNs with laparoscopic fluorescence imaging. Although researchers in the latter study used a near-infrared optical reporter, preparation of the agent required sterile compounding under the authority of the local pharmacist.

In our study, we confirmed that the attachment of a fluorescent imaging reporter did not alter the pharmacokinetic properties of tilmanocept. The in vitro binding studies showed that the attachment of the fluorophore did not alter the receptor affinity and nonspecific binding of tilmanocept, as measured by the mean dissociation constant and the fraction of nonspecific binding, respectively. A decrease in receptor affinity of Cy7 tilmanocept would decrease SLN extraction and therefore increase the probability of distal lymph node uptake. An increase in nonspecific binding would reduce the ability of Cy7 tilmanocept to enter the lymph channels and impede injection site clearance. The mouse study results showed rapid injection site clearance and SLN accumulation with ample fluorescent signal.

Tilmanocept belongs to a class of radiopharmaceuticals that accumulate at the target tissue via a receptor-mediated mechanism (30). The design strategy for tilmanocept (11) requires extremely high receptor affinity and a low molar dose that will not saturate the receptors within the SLN. This strategy permits the receptors to extract all of the tilmanocept flowing into the SLN. Complete extraction prevents tilmanocept from reaching the second lymph node in the chain. The mouse studies showed receptor-mediated binding to SLNs. In summary, the attachment of the near-infrared fluorophore Cy7 did not alter the receptor affinity and pharmacokinetics of tilmanocept. ^{99m}Tc-labeled Cy tilmanocept is a multireporter probe that exhibits the in vitro and in vivo requirements for receptor-targeted SLN mapping via nuclear and optical imaging.

Attachment of an optical imaging reporter to tilmanocept will expand the applications of the SLN concept. When combined with other advances in medical imaging, optically labeled tilmanocept offers the potential for SLN mapping without radioactivity. The development of intraoperative optical imaging (31) will enable wider dissemination of SLN mapping to hospitals without access to radiopharmaceuticals. This is especially true in developing countries, where only urban hospitals are equipped to handle radioactivity (32).

Unlike nuclear imaging reporters, which constantly emit photons and diminish in signal over time, optical imaging reporters only emit photons when properly illuminated. Consequently, ^{99m}Tc-labeled Cy7 tilmanocept and fluorine 18-labeled near-infrared tilmanocept (33) offer solutions to problems encountered at SLN mapping of cancers in locations such as the prostate, colon, and lung. For example, in preparation for robot-assisted prostatectomy, the surgeon can obtain a tomographic map of the patient's pelvic SLNs. This would be achieved with transrectal injection of dual-labeled tilmanocept into the prostate, followed by hybrid imaging with combined SPECT and computed tomography (CT) or combined positron emission tomography and CT. Preoperative imaging would guide the surgeon solely to the basins that contain the sentinel lymph. This SPECT/CT strategy has been proved to save operative time during SLN mapping (34). Because this strategy uses SLN mapping via fluorescence detection, scheduling of robotic surgery would be free of the time restrictions imposed by the nuclear reporter. A multimodal agent that uses radioactivity and fluorescence would play to the strength of both modalities: Nuclear imaging could be used to scan large volumes with high sensitivity, and fluorescence imaging could be used for detection within small spatial dimensions.

Acknowledgments: We thank the staff of the In Vivo Imaging Shared Resource of the UCSD In Vivo Cancer and Molecular Imaging Center: Jacqueline A. Corbeil, BS; Rosemarie G. Ramirez, BS; and Salman Farshchi-Heydari, BS. We thank Philip Stahl for his generous gift of the J774E cells and Jonathan Sorger of Intuitive Surgical and Robert F. Mattrey, MD, of the UCSD Radiology Department for their reviews and thoughtful discussions. We thank Roger Y. Tsien, PhD, for his guidance during the optical characterization of Cy7 tilmanocept.

Disclosures of Potential Conflicts of Interest: D.K.E. No potential conflicts of interest to disclose. **K.K.L.** No potential conflicts of interest to disclose. **D.J.H.** No potential conflicts of interest to disclose. **S.H.H.** No potential conflicts of interest to disclose. **W.C.E.** Financial activities related to the present article: none to disclose. Financial activities not related to the present article: is a consultant to Molecular Insight. Other relationships: none to disclose. **C.J.K.** Financial activities related to the present article: none to disclose. Financial activities not related to the present article: is a consultant to Janssen, GenProbe, Amgen, and Iris Personalized Medicine. Other relationships: none to disclose. **A.M.W.** Financial activities related to the present article: none to disclose. Financial activities not related to the present article: institution received a grant from and was compensated for travel and meeting expenses by Navidea Biopharmaceuticals. Other relationships: none to disclose. **D.R.V.** Financial activities related to the present article: none to disclose. Financial activities not related to the present article: sublicensed a patent to and receives royalties from Navidea Biopharmaceuticals; institution sublicensed a patent to and receives royalties from Navidea Biopharmaceuticals. Other relationships: none to disclose.

References

1. Morton DL, Wen D-R, Wong JH, et al. Technical details of intraoperative lymphatic mapping for early stage melanoma. Arch Surg 1992;127(4):392–399.
2. Krag DN, Weaver DL, Alex JC, Fairbank JT. Surgical resection and radiolocalization of the sentinel lymph node in breast cancer using a gamma probe. Surg Oncol 1993;2(6):335–339; discussion 340.
3. Giuliano AE, Kirgan DM, Guenther JM, Morton DL. Lymphatic mapping and sentinel lymphadenectomy for breast cancer. Ann Surg 1994;220(3):391–398; discussion 398–401.
4. Morton DL, Thompson JF, Essner R, et al. Validation of the accuracy of intraoperative lymphatic mapping and sentinel lymphadenectomy for early-stage melanoma: a multicenter trial—Multicenter Selective Lymphadenectomy Trial Group. Ann Surg 1999;230(4):453–463; discussion 463–465.
5. Turner RR, Ollila DW, Krasne DL, Giuliano AE. Histopathologic validation of the sentinel lymph node hypothesis for breast carcinoma. Ann Surg 1997;226(3):271–276; discussion 276–278.
6. Krag DN, Weaver D, Ashikaga T, et al. The sentinel node in breast cancer: a multicenter validation study. N Engl J Med 1998;339(14):941–946.
7. Veronesi U, Paganelli G, Viale G, et al. A randomized comparison of sentinel-node biopsy with routine axillary dissection in breast cancer. N Engl J Med 2003;349(6):546–553.
8. Faries MB, Morton DL. Surgery and sentinel lymph node biopsy. Semin Oncol 2007;34(6):498–508.
9. Lucci A, McCall LM, Beitsch PD, et al. Surgical complications associated with sentinel lymph node dissection (SLND) plus axillary lymph node dissection compared with SLND alone in the American College of Surgeons Oncology Group Trial Z0011. J Clin Oncol 2007;25(24):3657–3663.
10. Morton DL, Hoon DS, Cochran AJ, et al. Lymphatic mapping and sentinel lymphadenectomy for early-stage melanoma: therapeutic utility and implications of nodal microanatomy and molecular staging for improving the accuracy of detection of nodal micrometastases. Ann Surg 2003;238(4):538–549; discussion 549–550.
11. Vera DR, Wallace AM, Hoh CK, Mattrey RF. A synthetic macromolecule for sentinel node detection: (99m)Tc-DTPA-mannosyl-dextran. J Nucl Med 2001;42(6):951–959.
12. Wallace AM, Hoh CK, Vera DR, Darrah DD, Schulteis G. Lymphoseek: a molecular radiopharmaceutical for sentinel node detection. Ann Surg Oncol 2003;10(5):531–538.
13. Wallace AM, Hoh CK, Ellner SJ, Darrah DD, Schulteis G, Vera DR. Lymphoseek: a molecular imaging agent for melanoma sentinel lymph node mapping. Ann Surg Oncol 2007;14(2):913–921.
14. Leong SPL, Kim J, Ross MI, et al. A phase 2 study of (99m)Tc-tilmanocept in the detection of sentinel lymph nodes in melanoma and breast cancer. Ann Surg Oncol 2011;18(4):961–969.
15. Tokin CA, Cope FO, Metz WL, et al. The efficacy of tilmanocept in sentinel lymph node mapping and identification in breast cancer patients: a comparative review and meta-analysis of the ^{99m}Tc-labeled nanocolloid human serum albumin standard of care. Clin Exp Metastasis (in press).
16. Ellner SJ, Méndez J, Vera DR, Hoh CK, Ashburn WL, Wallace AM. Sentinel lymph node mapping of the colon and stomach using lymphoseek in a pig model. Ann Surg Oncol 2004;11(7):674–681.
17. Wallace AM, Hoh CK, Limmer KK, Darrah DD, Schulteis G, Vera DR. Sentinel lymph node accumulation of Lymphoseek and Tc-99m-sulfur colloid using a "2-day" protocol. Nucl Med Biol 2009;36(6):687–692.
18. Schaafsma BE, Mieog JS, Hutteman M, et al. The clinical use of indocyanine green as a near-infrared fluorescent contrast agent for image-guided oncologic surgery. J Surg Oncol 2011;104(3):323–332.
19. Silberstein JL, Derweesh IH, Kane CJ. Lymph node dissection during robot-assisted radical prostatectomy: where do we stand? Prostate Cancer Prostatic Dis 2009;12(3):227–232.
20. Rossi EC, Ivanova A, Boggess JF. Robotically assisted fluorescence-guided lymph node mapping with ICG for gynecologic malignancies: a feasibility study. Gynecol Oncol 2012;124(1):78–82.
21. Mujumdar RB, Ernst LA, Mujumdar SR, Lewis CJ, Waggoner AS. Cyanine dye labeling reagents: sulfoindocyanine succinimidyl esters. Bioconjug Chem 1993;4(2):105–111.
22. Vera DR, Hall DJ, Hoh CK, Gallant P, McIntosh LM, Mattrey RF. Cy5.5-DTPA-galactosyl-dextran: a fluorescent probe for in vivo measurement of receptor biochemistry. Nucl Med Biol 2005;32(7):687–693.
23. Hoh CK, Wallace AM, Vera DR. Preclinical studies of [(99m)Tc]DTPA-mannosyl-dextran. Nucl Med Biol 2003;30(5):457–464.
24. Diment S, Leech MS, Stahl PD. Generation of macrophage variants with 5-azacytidine: selection for mannose receptor expression. J Leukoc Biol 1987;42(5):485–490.
25. Munson PJ, Rodbard D. Ligand: a versatile computerized approach for characterization of ligand-binding systems. Anal Biochem 1980;107(1):220–239.
26. Scatchard G. The attractions of proteins for small molecules and ions. Ann N Y Acad Sci 1949;51(4):660–672.
27. Vera DR, Woodle ES, Stadalnik RC. Kinetic sensitivity of a receptor-binding radiopharmaceutical: technetium-99m galactosyl-neoglycoalbumin. J Nucl Med 1989;30(9):1519–1530.
28. van Dam GM, Themelis G, Crane LMA, et al. Intraoperative tumor-specific fluorescence imaging in ovarian cancer by folate receptor-α targeting: first in-human results. Nat Med 2011;17(10):1315–1319.
29. van der Poel HG, Buckle T, Brouwer OR, Valdés Olmos RA, van Leeuwen FWB. Intraoperative laparoscopic fluorescence guidance to the sentinel lymph node in prostate cancer patients: clinical proof of concept of an integrated functional imaging approach using a multimodal tracer. Eur Urol 2011;60(4):826–833.
30. Eckelman WC, Reba RC. The classification of radiotracers. J Nucl Med 1978;19(10):79–81.
31. Gioux S, Choi HS, Frangioni JV. Image-guided surgery using invisible near-infrared light: fundamentals of clinical translation. Mol Imaging 2010;9(5):237–255.
32. Keshtgar MRS, Zaknun JJ, Sabih D, et al. Implementing sentinel lymph node biopsy programs in developing countries: challenges and opportunities. World J Surg 2011;35(6):1159–1168; discussion 1155–1158.
33. Ting R, Aguilera TA, Crisp JL, et al. Fast 18F labeling of a near-infrared fluorophore enables positron emission tomography and optical imaging of sentinel lymph nodes. Bioconjug Chem 2010;21(10):1811–1819.
34. Warncke SH, Mattei A, Fuechsel FG, Z'Brun S, Krause T, Studer UE. Detection rate and operating time required for γ probe-guided sentinel lymph node resection after injection of technetium-99m nanocolloid into the prostate with and without preoperative imaging. Eur Urol 2007;52(1):126–132.